European Journal of Pharmaceutics and Biopharmaceutics 213 (2025) 114758

Contents lists available at ScienceDirect

European Journal of Pharmaceutics and Biopharmaceutics

journal homepage: www.elsevier.com/locate/ejpb

The role of organic acid counterions in modulating the *in-vitro* dissolution and permeability profiles of procaine salts

Paola Disisto [a,b], Laura Baraldi [a,b], Luca Fornasari [b], Irene Bassanetti [b], Valentina Mileo [b], Francesco Castagnini [b,d], Francesca Ferlenghi [d], Pietro Franceschi [e], Alessia Bacchi [a,c], Luciano Marchiò [a,c,*]

[a] *Dipartimento di Scienze Chimiche, della Vita e della Sostenibilità Ambientale, Università di Parma 43124 Parma, Italy*
[b] *Preclinical Analytics and Early Formulations Department, Chiesi Farmaceutici S.p.A., Largo Belloli, 43123 Parma, Italy*
[c] *Biopharmanet TEC, Tecnopolo Padiglione 33, Università di Parma 43124 Parma, Italy*
[d] *Department of Food and Drug, University of Parma 43124 Parma, Italy*
[e] *Fondazione Edmund Mach, 38098 San Michele all'Adige (TN), Italy*

ARTICLE INFO

Keywords:
Procaine
Organic acids
Dissolution
Permeability
Lipophilicity
Intermolecular interactions
Ion pair
Salification

ABSTRACT

Procaine, a widely used local anesthetic, suffers from slow onset and rapid degradation into *para*-aminobenzoic acid and diethylaminoethanol, resulting in a brief half-life and short duration of action. In this study, we investigate salification in order to modify dissolution rate and permeability without altering the chemical structure or using complex formulations. Six procaine salts with carboxylic acids and four with sulfonic acids were prepared and systematically evaluated in comparison with procaine hydrochloride, focusing on their *in-vitro* pharmacokinetic properties in two physiological conditions at pH 4.5 and 7.4. Dissolution rate studies showed that all procaine salts achieved complete dissolution within 30 min, while procaine reached 75 % dissolution and remained partially undissolved even after 2 h. In addition, permeability studies revealed a range of permeation values among the different procaine salts, in which sulfonate anions significantly improved the permeability of procaine by approximately 40 % to 70 %. Furthermore, a correlation between permeability and lipophilicity descriptors was assessed, with particular attention to ion pair stability, the lipophilicity of the counterion and the lipophilicity of procaine in its neutral form. Notably, salts with higher permeability, primarily sulfonates, exhibited less stable ion pairs, contributing to a more effective drug diffusion and a potential for faster onset and absorption of procaine. On the other side, carboxylic acids tend to confer a higher ion pair stability, inhibiting the membrane permeation. Our findings support the canonical model of passive permeability, suggesting that the neutral form of the drug can form in response to local environmental conditions near the membrane or within the transmembrane compartment. In this context, both the neutral form and the ion pair could contribute and play a role as a part of the equilibrium of partitioning across the membrane.

1. Introduction

Procaine is an active pharmaceutical ingredient (API) which has gained significant interest thanks to its versatility in the treatment of several diseases [1,2]. Originally discovered by Alfred Einhorn in 1905 as an aminoester local anaesthetic, procaine quickly emerged as a safer alternative to cocaine, primarily due to its more favourable effectiveness profile and reduced potential for abuse [3,4]. As an aminoester local anaesthetic, procaine exerts its effects by reversibly blocking nerve impulses by inhibiting sodium ion channels, thereby producing a temporary numbness and loss of sensation in a localized area [5]. This property has made procaine an invaluable tool in medical and dental procedures and anaesthesia, providing effective pain relief [6], while minimizing the risk of systemic toxicity associated with some other anaesthetics [7–9].

The molecular structure of procaine consists of an aromatic ring, which provides lipophilicity, rigidity and stability to the structure, attached to an amino group (–NH_2) and an ester group (–COO-) via an

* Corresponding author at: Dipartimento di Scienze Chimiche, della Vita e della Sostenibilità Ambientale, Università di Parma, 43124 Parma, Italy. Biopharmanet TEC, Tecnopolo Padiglione 33, Università di Parma, 43124 Parma, Italy.
E-mail address: luciano.marchio@unipr.it (L. Marchiò).

https://doi.org/10.1016/j.ejpb.2025.114758
Received 16 January 2025; Received in revised form 24 April 2025; Accepted 26 May 2025
Available online 26 May 2025

ethyl linkage (Fig. 1), therefore endowed with both hydrophobic and hydrophilic features [10].

The amino group plays a role in the anaesthetic properties of procaine, while the ester group is involved in its metabolism. Procaine undergoes hydrolysis by esterases, breaking down the compound into *para*-aminobenzoic acid (PABA) and diethylaminoethanol. The susceptibility of the ester group to hydrolysis influences the short duration of action of the drug (approximately 30 min) [11], which is one of its major limitations. Indeed, once hydrolyzed, the resulting products, such as PABA, can be further metabolized or excreted from the body [12], necessitating frequent re-administration for sustained pain relief or anaesthesia. This poses challenges in clinical settings, as repeated injections can be inconvenient for patients and may increase the risk of adverse events [13]. Hence, it is important to investigate strategies that prevent its rapid metabolism. For this purpose, patches [14], hydrogels [15], nanoparticles [16] and advanced drug delivery systems [17–19] were developed. However, these systems also have the drawback of insufficient stability, being burdensome for large-scale production, having exorbitant costs, or being too time-consuming [18].

Furthermore, procaine is known to exhibit poor penetration through biological barriers [20], particularly the blood–brain barrier. This limited ability to cross membranes hinders its application for central nervous system-related procedures. Improving the permeability and transport of procaine across biological barriers would expand its potential applications and enhance its effectiveness for various anaesthesia and pain management interventions [11].

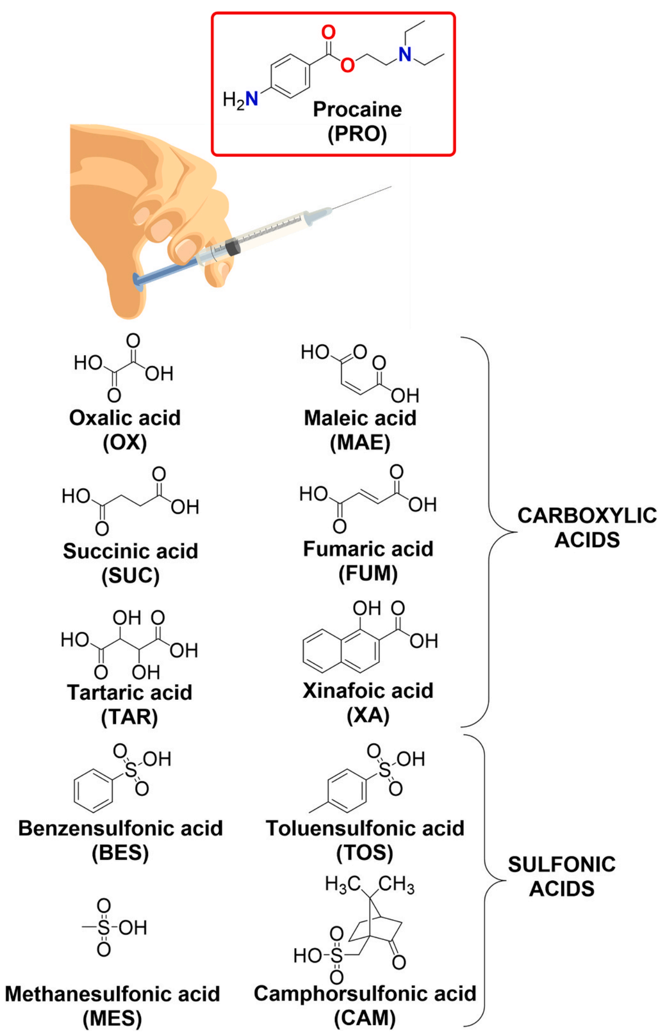

Fig. 1. Chemical structure of procaine free-base and acids used to obtain procaine salts.

Salification could modulate procaine absorption and help prevent its rapid metabolism into PABA and derivatives, which is essential for ensuring patient safety and mitigating potential toxicity concerns. This approach may enhance stability and extend the duration of action of the drug, effectively circumventing the traditionally slow onset time of procaine alone [21]. In the case of procaine salts, their absorption potential may be modulated depending on the chemical nature of the counterions engaged with the protonated procaine cation (PH^+) [22] and the surrounding aqueous environment. In solution, these species may form a variety of ionic assemblies or complexes, where multiple charged entities combine, collectively affecting properties of the drug, including lipophilicity, dissolution rate, and permeability [23–25]. Indeed, counterions may exert a protective influence on the parent drug, preventing its proneness to hydrolysis and facilitating a quicker absorption into the bloodstream, leading to a more rapid onset of action. This is particularly beneficial in clinical scenarios where swift anaesthesia is crucial.

Yet, the specific influence of a certain range of organic counterions on the permeability behaviour of procaine salts remains relatively unexplored in the literature, while for other drugs like hydrochlorothiazide, some works in the literature assessed the importance of the intermolecular interactions in driving the solubility and the membrane diffusion [26–28]. This project represents an extension of our earlier research on benzocaine salts, where dissolution rate and permeability were widely examined, laying the groundwork for the current work into procaine salts [29]. In that context, the low p*K*a of the protonated form of benzocaine (p*K*a $BH^+ = 2.29$) made lipophilicity *vs* pH studies not feasible, highlighting the need for further exploration with another local anesthetic such as procaine. The purpose of this investigation is to identify the most appropriate salts to overcome procaine limitations and to assess how their lipophilicity influences the ability to permeate plasma membranes.

In this study, eleven procaine salts were prepared by pairing procaine with different counterions, including chloride, carboxylates (6 adducts), and sulfonates (4 adducts), which provide a sufficiently wide array of chemical structures and properties. The salification agents (acids) were selected in order to explore a range of lipophilicity, while preserving a potential ion pair stability, following crystal engineering principles. Carboxylate and sulfonate groups were chosen for their compatibility with procaine, enabling intermolecular interactions through hydrogen bonds. Xinafoic acid, *p*-toluenesulfonic acid, and benzenesulfonic acid additionally introduce π-π interactions due to their aromatic systems. The selected acids are also generally recognized as safe (GRAS) counterions, ensuring biocompatibility [30–32]. Specifically, procaine hydrochloride (PRO-HCl), procaine oxalate (PRO-OX), procaine mesylate (PRO-MES), procaine besylate (PRO-BES) and procaine tosylate (PRO-TOS) were already known in the literature, even if not completely characterized [22,33]. On the other hand, procaine maleate (PRO-MAE), procaine xinafoate (PRO-XA), procaine fumarate (PRO-FUM), procaine succinate (PRO-SUC), procaine tartrate (PRO-TAR), procaine camphorsulfonate (PRO-CAM) were new systems. We initially assessed the molecular structures of the ion pair adducts through single crystal X-ray diffraction. In a second stage, dissolution rate and permeability were evaluated in two different buffer solutions, selected to mimic physiologically relevant conditions: pH 4.5, representing the acidic microenvironment of certain biological fluids, and pH 7.4, corresponding to extracellular systemic conditions. The salts exhibited both enhanced dissolution rate and permeability compared to procaine free-base. A crucial aspect in permeability studies is the bilayer membrane crossing. Hence, the lipophilicity profile of the species is expected to play a pivotal role in either facilitating or hindering the permeation of procaine across the lipid membrane that separates two aqueous environments [34]. For this reason, lipophilicity profiles were assessed over a broader pH range, spanning approximately from 4 to 12, to capture variations in partitioning behavior as a function of pH. Two lipophilicity parameters were evaluated: the lipophilicity of the counterion ($\log P_{counterion}$) and *diff*log*P*, that reflects the influence of ionization on the intermolecular and intramolecular interactions of a solute and partitioning on a biphasic system, according to the established methodology outlined by Caron and Malvezzi [35,36]. The latter was parametrized by the difference (*diff*log*P*) between the partition coefficient of the ionized species PH^+ ($\log P^I$), determined at acidic pH, and the one of the neutral species ($\log P^N$), assessed at alkaline pH. Consequently, as reported also in the works of Scherrer and Malvezzi, variations in *diff*log*P* values reflect changes in the stability of the ion pairs, when the ionic species involved are relatively hydrophobic [35,37]. In general, the characterization of ion pairs in solution is well-documented in the literature, often taking into account aggregation phenomena that can occur with sufficiently hydrophobic species [38–40]. For all the systems studied, the outcomes revealed *diff*log*P* and $\log P_{counterion}$ to be orthogonal parameters, which are able to catch different facets of the interaction phenomena occurring in solution between the ionic species involved, and they both showed a positive correlation with permeability. The salification approach results in improved regulation of the *in-vitro* permeability of procaine, ensuring the necessary dissolution rate of the drug, which are crucial factors for achieving more promising effects.

2. Materials and methods

Procaine free-base was used as received from Tokyo Chemical Industry Co., Ltd. (APAC). Hydrochloric acid 37 %, oxalic acid, maleic acid, xinafoic acid, fumaric acid, succinic acid, (*2R,3R*)-(+)-tartaric acid, methanesulfonic acid, p-toluenesulfonic acid, benzenesulfonic acid, (*1S*)-(+)-10-camphorsulfonic acid, PBS tablets, ethyl acetate (EtOAc), absolute ethanol (EtOH abs), methyl *tert*-butyl ether (MTBE), Acetonitrile (ACN), water, acetic acid, boric acid, phosphoric acid, sodium hydroxide (NaOH) pellets, potassium chloride (KCl) and ammonium acetate were purchased from MERCK-Sigma Aldrich. Dimethylsulfoxide (DMSO) was supplied by Alfa Aesar GmbH (Karlsruhe, Germany) and *n*-octanol (*n*-oct) was supplied by Chem-Lab NV (Zeldegem, Belgium). Ultra-pure water was dispended by a Arium confort purification system (Sartorius AG, Gottingen, Germany). Solvents were commercially available and used without any other purification. Permeapad barrier used for permeability studies was purchased by InnoME GmbH (Espelkamp, Germany).

2.1. Procaine salts preparations

Slurry crystallization was used to prepare the whole set of procaine salts. The salt was obtained by adding an equimolar amount of procaine free-base and counterions (1:1 stoichiometry) in presence of EtOAc as solvent in a closed vial (concentration of 50 mg/mL) at room temperature (RT). In these reaction conditions, PRO-HCl, PRO-OX, PRO-MAE, PRO-MES, PRO-TOS, PRO-BES, PRO-CAM instantly precipitated as a white solid, which was left in slurry for 24 h and then kept at 0 °C to ensure quantitative precipitation. In the end, the suspension was filtered, washed with EtOAc and dried. Yield (%): PRO-HCl (69 %), PRO-OX (91 %), PRO-MAE (88 %), PRO-MES (83 %), PRO-TOS (80 %), PRO-BES (80 %), PRO-CAM (75 %).

The same procedure was used for PRO-XA, PRO-FUM, PRO-SUC, even if using MTBE as solvent. In these conditions, single crystals suitable for X-ray structural analysis were obtained by slow evaporation of the solvent. Yield (%): PRO-XA (78 %), PRO-FUM (87 %), PRO-SUC (94 %).

PRO-TAR was the only salt for which a 1:1 stoichiometry did not lead to the successful formation of the desired salt in a crystalline form under any conditions. Consequently, a 2:1 ratio of PRO:TAR was adopted, by mixing tartaric acid and two equivalents of procaine free-base in EtOH abs (concentration of 50 mg/mL). The mixture was heated at 40 °C until complete dissolution of the solid and rapidly cooled to 5 °C. After 24 h, the precipitated powder was filtered, washed with cold EtOH abs and dried (yield 72 %).

The compounds were characterized by X-ray powder diffraction (XRPD) (Fig. 2), differential scanning calorimetry (DSC) (see Supporting Information, Fig. S6), single crystal X-ray diffraction (SC-XRD) (Figs. 3-5) and ^1H NMR (see Supporting Information, Fig. S7-S17). The salts were stored under ambient conditions (25 °C/65 %RH) for over two years without requiring special storage conditions. During this period, no visible and substantial changes were observed (e.g., discoloration, hygroscopicity, or phase transformation), and periodic XRPD, DSC, TGA and ^1H NMR analyses revealed neither significant alteration in the solid form, nor chemical degradation, confirming the intrinsic solid-state stability of the salts.

2.2. Single-crystal X-ray diffraction (SC-XRD)

Crystals of procaine salts suitable for SC-XRD analysis were obtained alternatively in slurry from synthesis suspensions or from slow evaporation of solution of samples achieved by crystallization solvents. Single crystal data were collected at 220 K with a Bruker D8 Venture diffractometer equipped with a Photon II detector, using CuKα (λ = 1.54184 Å) or MoKα (λ = 0.71073 Å) microfocus radiation sources. The intensity data were integrated from several series of exposure frames covering the sphere of reciprocal space. Data reductions were performed with APEX4. Absorption corrections were applied using the program SADABS [41].

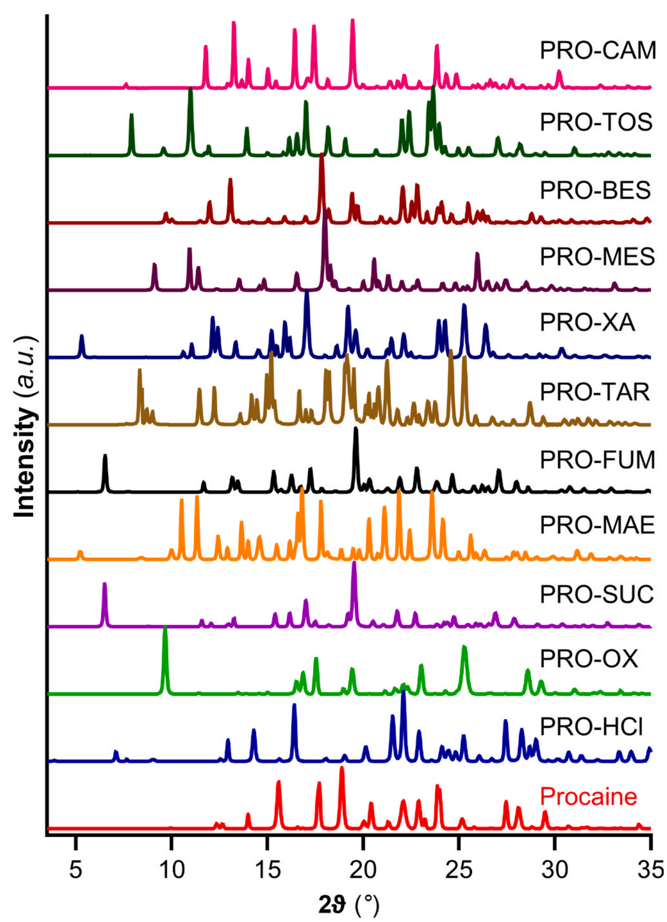

Fig. 2. Superimposition of the powder X-ray diffraction experimental patterns of (a) Procaine free-base, (b) Procaine Chloride (PRO-HCl), (c) Procaine Oxalate (PRO-OX), (d) Procaine Succinate (PRO-SUC), (e) Procaine Maleate (PRO-MAE), (f) Procaine Fumarate (PRO-FUM), (g) Procaine Tartrate (PRO-TAR), (h) Procaine xinafoate (PRO-XA), (i) Procaine Mesylate (PRO-MES), (l) Procaine Besylate (PRO-BES), (m) Procaine Tosylate (PRO-TOS), (n) Procaine Camphorsulfonate (PRO-CAM).

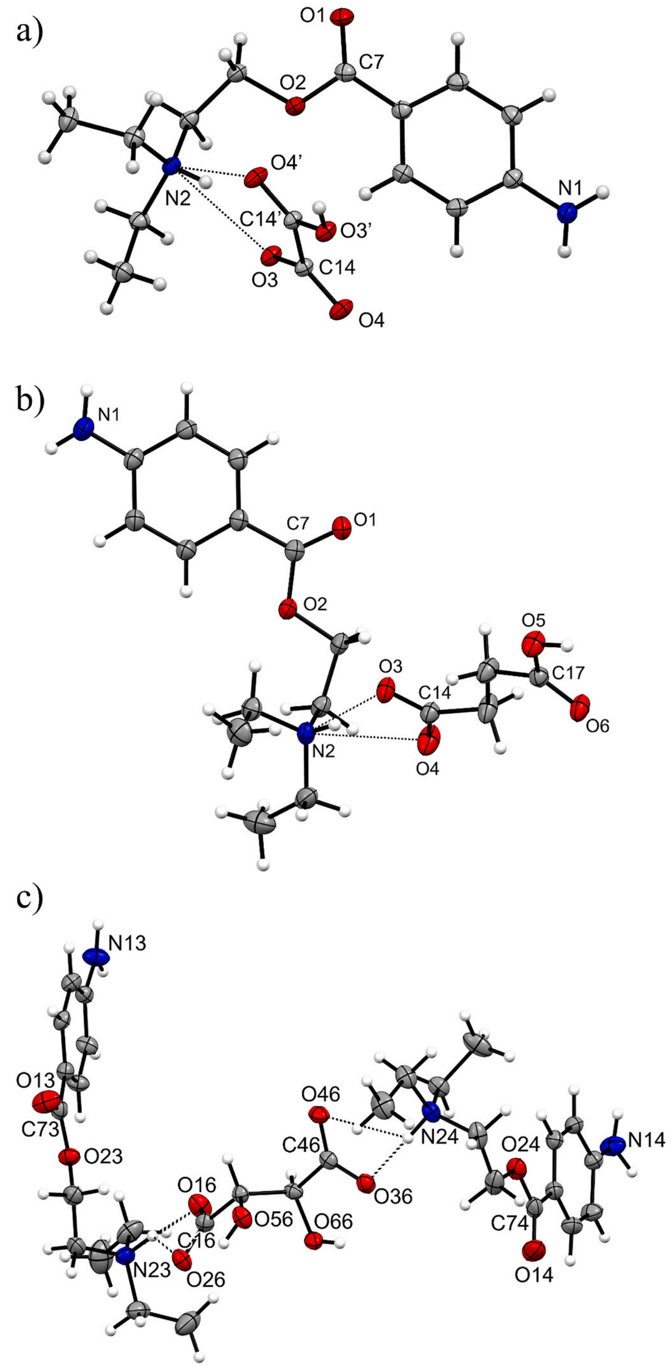

Fig. 3. Molecular structure of a) PRO-OX, b) PRO-SUC, c) PRO-TAR. Thermal ellipsoids are depicted at the 30% probability level. Dashed lines represent hydrogen bonds. a) In PRO-OX, two half oxalate monoanion are situated on an inversion center. Only one monodeprotonated oxalate anion is depicted for clarity. Symmetry code: (') 1-x, 1-y, 2-z. b) In PRO-SUC, the asymmetric unit is reported, which lays one protonated procaine molecule and one monodeprotonated succinate. c) In PRO-TAR, only three fragments are depicted for clarity, to show the bisdeprotonated nature of tartrate.

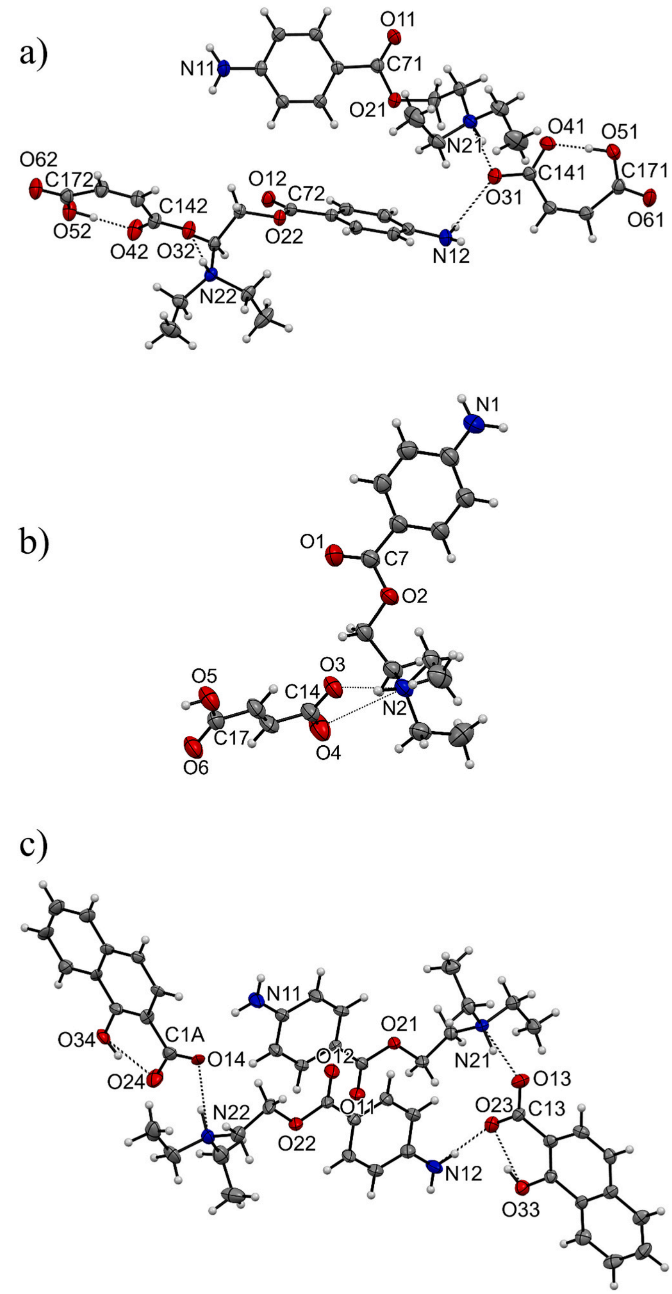

Fig. 4. Molecular structure of a) PRO-MAE, b) PRO-FUM, c) PRO-XA. In PRO-MAE and PRO-XA, two protonated procaine molecules and two monodeprotonated anions comprise the asymmetric unit. Thermal ellipsoids are depicted at the 30% probability level. Dashed lines represent hydrogen bonds.

The structures were solved by intrinsic phasing with the program SHELXT [42]. Fourier analysis and refinement were performed by the full-matrix least-squares methods based on F^2 using SHELXL-2017 [43] implemented in Olex2 software (version 1.3) [44]. Non-H atoms were refined anisotropically. For all structures, except PRO-XA, the hydrogen atoms bound to the nitrogen or oxygen atoms were located from the difference Fourier map and they were refined. The remaining H atoms were placed in calculated positions and refined with a riding model. Crystallographic data can be found in Supplementary Materials. CCDC 2415139-2415148 contains the supplementary crystallographic data for this paper. Hirshfeld surface (HS) analysis were calculated using the CrystalExplorer21 program [45,46]. HS properties were investigated to provide a thorough description of the interactions occurring between protonated procaine (PH^+) and the various anions. Fingerprint plots were used to analyze in detail the type of interactions occurring between PH^+ and its surroundings, including anions or symmetry related PH^+ molecules. Some crystal structures were characterized by the presence of disordered fragments. During the HS analysis, these fragments were considered with their fractional occupancies.

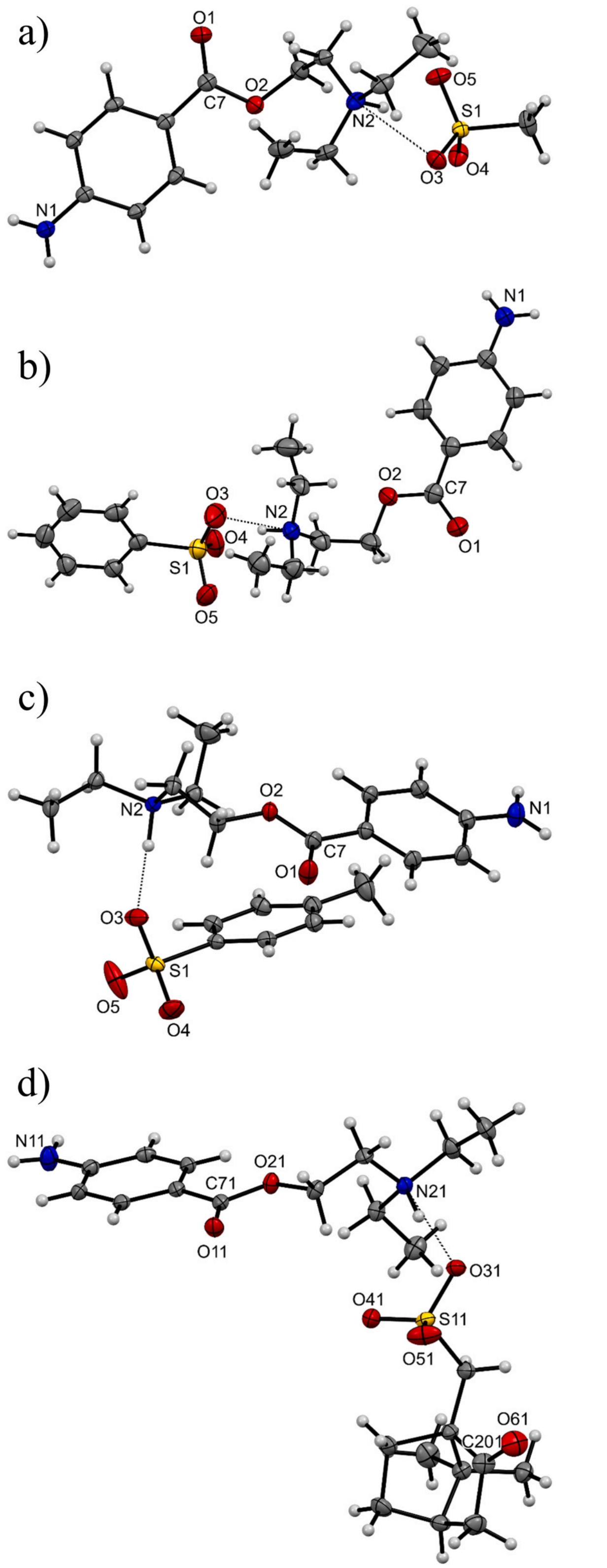

Fig. 5. Molecular structure of a) PRO-MES, b) PRO-BES, c) PRO-TOS, d) PRO-CAM. The reported asymmetric units lay one protonated procaine molecule and one deprotonated sulfonate anion. In PRO-CAM, only two fragments are depicted for clarity, to show the interaction between PH^{+} and the anion. Thermal ellipsoids are depicted at the 30 % probability level. Dashed lines represent hydrogen bonds.

2.3. *X-ray powder diffraction (XRPD)*

The crystalline state of the samples was investigated by X-ray powder diffraction (XRPD) with an Emyrean Panalytical (UK) V 2.0 instrument equipped with Cu radiation source. Samples were placed on zero background sample holders. The measurements were performed in reflection mode with 2Theta scans from 1.5 to 45°, step size 0.02°, soller slit 0.02 rad, divergence slit 1/8°, antiscatter slit 1/4°.

2.4. *Thermal methods*

Differential Scanning Calorimetry (DSC) analyses were performed using a routinely calibrated TA Instruments differential scanning calorimeter Discovery equipped with a computer analyzing system (TRIOS). Indium standard and a sapphire disk were used for temperature/enthalpy calibration and heat capacity calibration, respectively. The system was equipped with a refrigerated cooling system (RCS90) accessory under a dry nitrogen purge (50 mL/min). About 1–5 mg of each sample was placed into a Tzero Aluminum hermetic DSC pan covered with a lid. The sample cell was equilibrated at 0 °C and heated under a nitrogen purge (50 mL/min). All samples were given similar thermal histories by linearly heating to 300 °C at a heating rate of 10 °C/min.

2.5. *^{1}H NMR*

NMR spectra were recorded on a Bruker Avance NEO 400 MHz spectrometer equipped with a Prodigy BBO-H&F 5 mm cryoprobe (nitrogen) at a temperature of 298 K. Chemical shifts (δ) are reported in ppm relative to residual solvents signals for ^{1}H NMR. Coupling constants (*J* values) are given in hertz (Hz), and multiplicities are reported using the following abbreviation: s, singlet; d, doublet; t, triplet; q, quartet; m, multiplet; br, broad. DMSO-d_6 deuterated solvent used has been purchased from Merk.

2.6. *Dissolution rate studies*

An *in-vitro* dissolution rate assay was performed on procaine salts using an acetate buffer solution (pH 4.5) and PBS buffer (pH 7.4) as dissolution mediums at room temperature. To evaluate the dissolution kinetics at different time points, 8 suspensions were prepared for every compound at a concentration of 1 mg/mL of procaine, covering different check point (0, 5, 10, 20, 30, 40, 60, 120 min). A sample was also withdrawn after 24 h, in order to ensure the molecular integrity of procaine. For each suspension, 200 µL were withdrawn and filtered by RC Membrane Syringe Filters 0.22 µm, diluted in 1:10 ratio with ACN: H_2O 30:70 and injected into LC/UV/MS system. Each salt was tested in triplicate. These studies were conducted with the aim to quantify the procaine concentration in solution as a function of the time, generating a dissolution rate curve. Ultra-high-performance liquid chromatography with ultraviolet detection (UHPLC-UV) was used for quantitative analysis of the dissolved procaine which absorbs UV-light in the range of 200–290 nm with an absorbance maximum at 273 nm. UHPLC-UV analysis was conducted on a Waters Acquity UPLC system (Milford, MA, USA) that was connected to a diode array detector and equipped with a reversed phase Kinetex® EVO C8 LC column (100 × 2.1 mm; particle size 1.7 µm; pore size 100 Å, Phenomenex®). The mobile phase consisted of 25 mM of ammonium formate buffer (pH 3) and 0.1 % formic acid in acetonitrile, the flow rate was 0.5 mL/min and the column oven was set to 50 °C. The injection volume was 2 µL. This UHPLC-UV method was applied uniformly for both salts and procaine free-base.

2.7. *Permeability studies*

To investigate the passive diffusion of procaine salts, an *in-vitro* permeability experiment was carried out using a Permeapad barrier [47] with 96-well plate. Similarly to dissolution studies, the experiments were conducted in two different buffer systems: PBS pH 7.4 to simulate extracellular conditions and acetate buffer pH 4.5 to assess permeability under mildly acidic conditions. Each well was equipped with a donor compartment and an acceptor compartment, separated by an artificial membrane of phosphatidylcholine. Before starting the permeability experiment, each salt sample was first completely dissolved in the respective buffer at a concentration of 1 mg/mL. Afterwards, 200 μL of the resulting solution of sample were placed in the donor compartment, while 400 μL of pure buffer were added in the acceptor compartment. The plate was kept at room temperature and covered for the whole duration of the experiment to ensure the integrity of the membrane. For every time check (0, 15, 30, 60, 120, 240, 360, 480 min), the procaine concentration within the acceptor compartment was monitored withdrawing sample of 10 μL, then diluted 1:10 with ACN:H_2O 30:70 and injected into LC/UV/MS system. Eventually, 10 μL of fresh buffer were added back into the acceptor compartment in order to not alter its volume and concentration. Each permeability assay was carried out in triplicate for each salt. Ultra-high-performance liquid chromatography with ultraviolet detection (UHPLC-UV) was used for quantitative analysis of the dissolved drug which absorbs UV-light in the range of 200–290 nm with an absorbance maximum at 273 nm. UHPLC-UV analysis was conducted on a Waters Acquity UPLC system (Milford, MA, USA) that was connected to a diode array detector and equipped with a reversed phase Kinetex® EVO C8 LC column (100 × 2.1 mm; particle size 1.7 μm; pore size 100 Å, Phenomenex®). The mobile phase consisted of 25 mM of ammonium formate buffer (pH 3) and 0.1 % formic acid in acetonitrile, the flow rate was 0.5 mL/min and the column oven was set to 50 °C. The injection volume was 2 μL. This UHPLC-UV method was applied uniformly for both procaine free-base and its salts. Apparent Permeability (P_{app}) was estimated using the method introduced by Tzanova et al [48].

2.8. ProcaineH$^+$ pKa determination

ProcaineH$^+$ (PH$^+$) p*K*a was determined by spectrophotometric method in ionic strength adjusted (ISA) water (0.15 M KCl), under a nitrogen atmosphere and at 25.0 ± 0.5 °C employing a Sirius T3^{TM} instrument (P-Ion Inc. Ltd., Forrest Row, UK), which allows both pH- and UV-metric determination of p*K*a values [49]. Sirius T3Control and SiriusT3Refine software (v. 1.1.3.0) were employed for instrument control, and for the non-linear fitting of the UV absorbance *vs* pH curves by Target Factor Analysis, respectively [50]. p*K*a values were measured as triplicates.

2.9. LogD determination by shake-flask method

Experimental Log*D* values for each procaine salt in the pH range 4.2–11.6 were determined at room temperature (rt, 21.0 ± 0.5 °C) by the shake-flask method. Briefly, Britton-Robinson aqueous universal buffer (BRB) solutions at n = 11 different pH levels were prepared, by combining suitable volumes of acidic (acetic acid, boric acid, and phosphoric acid) and basic (NaOH) components [51]; ionic strength (μ_F) was corrected to 0.15 M by adding an appropriate amount of KCl. For each pH level, *n*-oct and BRB buffer were mutually saturated by overnight stirring.

2 mg of each procaine salt were weighted in a glass vial and completely dissolved in the pre-saturated organic or buffered phase, according to the expected solubility, to a concentration of 0.5–1 mg/mL

The solution was split in n = 4 vials, then the other pre-saturated phase was added and the biphasic samples were kept under stirring (2 h, 200 rpm, RT) to reach partition equilibrium.

Two different *n-oct*/BRB buffer ratios (*i.e.*, 150:300 and 100:400 μL) were tested in duplicates, for a total of n = 4 samples; at the end of partitioning time, partition phases were centrifuged (13000 rpm, 10 min, RT), manually separated, diluted with methanol and analyzed by HPLC-UV.

Diluted phases were eluted isocratically on an Inertclone 5 μM ODS-2 column 150 Å, 150 x 4.6 mm (Phenomenex, Torrance, USA); eluent A: acetonitrile; eluent B: 1 mM ammonium acetate, pH 7.0; 20 %A:80 %B; flow rate: 0.8 mL/min. Absorbance wavelength was set at 290 nm.

The distribution coefficient *D* was calculated as the area ratio of procaine peak in *n*-oct and aqueous phase.

The solver routine of Microsoft Excel 365 (Microsoft Corp., USA) was used to obtain logP^N, logP^I and *diff*log*P* parameters by fitting experimental log*D vs* pH curves to the equation:

$$logD = log\left(P^N + P^I 10^{pKa-pH}\right) - \log\left(1 + 10^{pKa-pH}\right)$$

which describes the partitioning behavior of a monoprotic base incorporating the partitioning of the ion pair[52]. The experimental value of p*K*a PH$^+$, determined as reported in paragraph 2.8, was employed as a seed value in the calculation [51].

3.1. Correlation analysis

Pearson correlation analysis between p*K*a, lipophilicity parameters and apparent permeability was performed in R [53]. The results were visualized in graphical form relying on the corrplot package [54].

4. Results and discussion

4.1. Solid state characterization of salts

Procaine salts were prepared by solvent-assisted techniques and, after purification, they were characterized by XRPD, DSC (see Fig. 2 and Supporting Information Fig. S6), SC-XRD (See Figs. 3-5) and ^{1}H NMR (Supporting Information, Fig. S7-S17). Following the assessment of the ion pair stoichiometry and of the structural features, we performed dissolution rate studies, permeability tests and *diff*log*P* measurements, with the aim of obtaining a structure–property relationship.

While procaine chloride had been previously documented in the literature, including its single crystal structure [55], the remaining salts were not structurally characterized.

Solid forms with a unique and crystalline XRPD pattern were isolated from salt formation experiments for all compounds. The overlay of the novel identified patterns together with that of procaine free-base is reported in Fig. 2.

Moreover, Figs. S6-S16 in the Supporting Information provide a comprehensive solid-state characterization of the pure starting materials (procaine and counterions), their physical mixtures, and the synthesized salts. The distinct diffraction patterns and thermal behaviors confirm that the salts crystallize in new solid phases, different from both the individual components and their physical mixtures. The DSC thermograms exhibited a distinctive and sharp endothermic event that can be associated with the melting of the corresponding salt and coupled with TGA confirms that all the solid forms are anhydrous. Additionally, thermal analysis (DSC and TGA) allows to further assess their thermal behavior and physicochemical stability as a function of the temperature. Thermogram profiles indicate that most procaine salts exhibit thermal stability up to at least 150–180 °C, with sulfonate salts (PRO-MES, PRO-BES, PRO-TOS, and PRO-CAM) generally demonstrating higher decomposition temperatures (200–250 °C), suggesting greater thermal resilience. Conversely, carboxylate salts (PRO-OX, PRO-SUC, PRO-MAE, PRO-FUM, PRO-TAR) tend to show weight loss at slightly lower temperatures (~180–200 °C). PRO-XA, which starts to decompose around 150 °C, appears to be the least thermally stable among the salts analyzed. These results highlight distinct thermal behaviors depending on the nature of the counterion. Furthermore, ^{1}H NMR confirmed the chemical integrity of the entities involved, excluding potential impurities of degraded products. The absence of any peaks related to solvent residues in the ^{1}H NMR spectra confirmed that all the solid forms were not solvates (see Supporting Information Fig. S17-S27). Nevertheless, through ^{1}H NMR we could not exclude the presence of hydrate forms, due to water residues into the deuterated solvents. The confirmation of the stoichiometry and the absence of solvent crystallization, including water, was obtained from the SC-XRD analysis (see Figs. 3-5). The comparison between the observed solid forms with the calculated pattern from the single crystal structures was reported in the Supporting Information Fig. S1-S2.

4.2. Crystallographic analysis of procaine salts

Procaine hydrochloride (PRO-HCl) can be considered as the simplest among the ion pairs reported in this work, as the anion comprised a monoatomic species (Cl^-). The structure of PRO-HCl was previously reported [55] and it will not be described here. The crystal structures of the various compounds show that neither hydrate nor solvate forms were obtained and they provide details of the interactions between the procaine in its protonated form (PH^+) and its anionic counterpart, which represent a fundamental aspect for the modulation of the pharmacokinetic profile of the adducts. In all systems, the procaine molecule is protonated on the aliphatic amino group and the anions act as hydrogen bond acceptor towards the protonated quaternary amino group of PH^+. According to the molecular structures, it is evident that the stoichiometric ratio between protonated procaine (PH^+) and the anion is 1:1 for the whole set of salts (PH^+: anion$^-$), according to the presence of monodeprotonated anions. The only exception is represented by PRO-TAR, where the tartrate anion is bisdeprotonated, resulting in a 2:1 stoichiometry ($2PH^+$: anion^{2-}): the compound of 1:1 stoichiometry could not be obtained experimentally despite the equimolar proportions of drug and counterion used.

The 1:1 stoichiometry and salt formation is expected with relatively strong monoprotic sulfonic acids (methanesulfonic acid: pKa = -1.86 [56]; benzenesulfonic acid: pKa = -2.80 [57]; p-toluenesulfonic acid: pKa = -1.34 [56]; camphorsulfonic acid: pKa = 1.20 [56]). On the other hand, biprotic carboxylic acids could potentially undergo two deprotonation events hence yielding a 2- charged anion. Interestingly, the mono-deprotonation does not occur only with tartaric acid, even using an equimolar amount of the components. A tentative explanation for the tartaric acid behavior can be found by inspecting the pKa values of the various acids. Indeed, tartaric acid is the second most acidic among the dicarboxylic acids discussed in this work as far as the pKa_2 is concerned, with the oxalic acid being the most acidic (oxalic acid: pKa_1 = 1.25, pKa_2 = 4.14; succinic acid: pKa_1 = 4.21, pKa_2 = 5.64; tartaric acid: pKa_1 = 2.89, pKa_2 = 4.40; maleic acid pKa_1 = 1.94 pKa_2 = 6.22; fumaric acid pKa_1 = 3.03, pKa_2 = 4.54) [56]. Tartaric acid also has pKa_1 and pKa_2 values that are close to each other with a difference of 1.51. This results in a limited pH range in which the mono-deprotonated species is present, which, combined with the low value of pKa_2, may facilitate the formation of the species with a stoichiometry of PH^+:tartrate^{2-} in a 2:1 ratio. On the other hand, oxalic acid has a wide pH range in which the monodeprotonated species is present, due to the large difference between pKa_1 and pKa_2 (2.89), and this could promote the formation of the species with a 1:1 stoichiometry between PH^+ and Oxalate$^-$. This situation is particularly evident for succinic acid, maleic acid and to a lesser extent for fumaric acid (Fig. S3). Interestingly, the asymmetric unit of PRO-MAE and PRO-XA salts comprise two symmetry-independent procaine molecules and two symmetry-independent counterion molecules, connected via hydrogen bonds, while PRO-TAR comprises four PH^+ molecules and two^{2-} tartrate molecules. The tartrate^{2-} species directly interacts via hydrogen bonds with four PH^+ cations. Details of the crystal packing showing the cation and anion arrangement is reported in the Supporting Information Fig. S4.

As far as the sulfonate salts are concerned, the asymmetric unit of PRO-MES, PRO-BES, PRO-TOS comprise a PH^+ moiety and an anion. Conversely, in PRO-CAM two symmetry-independent moieties characterize the asymmetric unit, Fig. 5. Details of the crystal packing are reported in Supporting Information Fig. S5. A comprehensive description of the interaction occurring between the PH^+ cations and the surrounding molecules (carboxylate or sulphonate anions as well as symmetry related PH^+ moieties) was performed through the Hirshfeld surface analysis (Supporting Information Figs. S28-S43). According to the fingerprint plots, all of the systems are characterized by a marked cusp associated to the hydrogen bond involving the protonated tertiary amino group of procaine and the oxygen atom of a carboxylate group or of a sulfonate group. To this cusp there is also the contribution of the hydrogen bond formed by the aromatic NH_2 group and the carboxylate moieties or the C=O group of symmetry related PH^+ molecules (for the carboxylate anions) and the oxygen atoms of sulfonate groups (for the sulfonate anions). A second type of interaction involves the carbonylic oxygen atom of PH^+ that acts as hydrogen bond acceptor. This second interaction is more evident for the PRO-OX, PRO-FUM, PRO-SUC and PRO-XA systems and less evident for the salts comprising the sulfonate anions. Indeed, in the case of sulfonate anions the carbonyl of PH^+ interacts with aliphatic or aromatic CH groups. A large part ($>$ 50 %) of the interactions exchanged by PH^+ involves the hydrogen atoms of PH^+ with the hydrogen atoms of the surrounding molecules. The three interactions briefly outlined above are associated to the three main cusps that are present in the fingerprint plots for all of the systems.

4.3. Analysis of lipophilicity profiles (logD vs pH) of procaine salts

The lipophilicity index, log$D$, represents the partition coefficient of a compound in a biphasic system, normally composed by an organic phase (*n*-octanol) and an aqueous phase at a specific pH. It reflects the balance between hydrophilicity and lipophilicity, influenced by the ionization state of the molecule. This is a crucial parameter to consider for assessing the pharmacokinetic profile of a drug, as it affects key properties such as passive permeability through biological membrane and distribution volume. Therefore, the lipophilicity of the neutral form of a compound is expressed by the log$P$, while the lipophilicity at a certain pH, based on the ionization percentage of the compound, is represented by the logD_{pH}.

In this context, standard experimental log$D$ *vs* pH profiles were employed to explore the partitioning behavior of procaine salts and to evaluate how the experimental lipophilicity of procaine varies depending on the specific salt formed, reflecting the influence of the different counterions involved.

In general, monoprotic bases, such as procaine, partition in two forms: neutral (logP^N) and ionized (logP^I) species often with a log$P$ difference up to 3–4 units [58]. It is generally expected that the neutral form of a compound exhibits a higher lipophilicity with respect to the corresponding ionic specie due to the presence of net charges in the latter. Hence logP^N is usually greater than logP^I. Thus, as detailed in the Materials and Methods section, fitting of experimental lipophilicity profiles (log$D$ *vs* pH) to the theoretical equation describing partitioning behavior, allows the determination of two lipophilicity parameters, namely logP^N, logP^I together with the pKa of the ionizable group. As shown in the representative lipophilicity profile reported in Fig. 6, logP^N $>$ logP^I and the log$D$ curve increases with pH with a sigmoidal shape (see Fig. S44 and Table S4-6 in Supporting Information for the complete log$D$ *vs* pH profiles and values for every procaine salt). From the values of logP^I and logP^N it is possible to determine the lipophilicity as a function of pH. The difference between the log$P$ of the neutral and ionized forms defines the parameter *diff*log$P$ which, in the family of lipophilicity profiles for the series of procaine salts, allows an estimate of the relative stability of the ion pair formed between the protonated base and salt counterions. However, since the buffer solutions at different pH contain multiple counterions mimicking the physiological ionic environment, the *diff*log$P$ reflects not only the stability of the procaine-counterion pair but also the collective interactions of procaine within this intricate ionic network [34]. Importantly, since for every pH level, the buffer composition is constant, the observed effects on the partitioning of the drug

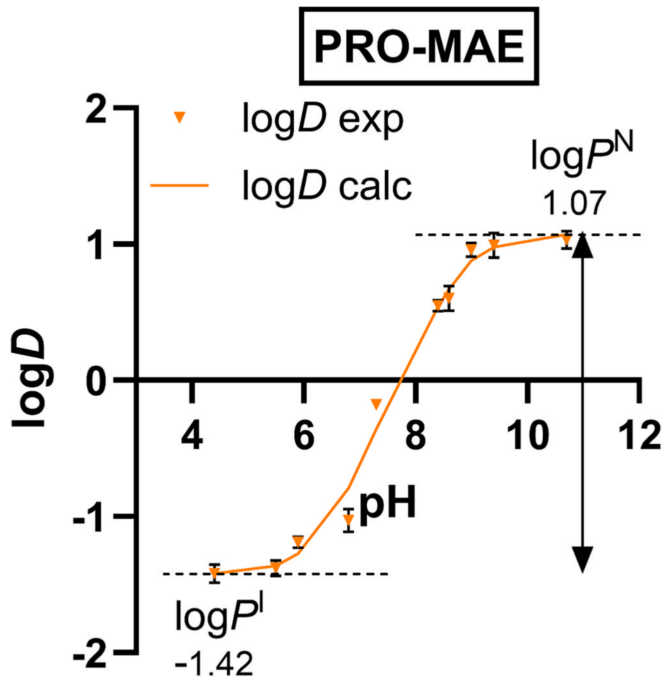

Fig. 6. Logd *vs* pH profile for the representative salt PRO-MAE. Reported are mean experimental logD values (logD exp) together with their SD (n = 3) interpolated by fitting curve (See Materials and methods for equation).

behavior can be attributed primarily to the nature of the specific counterion in the procaine salt. This approach enables a focused analysis of how the choice of counterion influences the lipophilicity of procaine and, consequently, its permeability.

Table 1 summarizes lipophilicity parameters obtained for the different procaine salts by fitting of shake-flask log*D* *vs* pH lipophilicity profiles. p*K*a PH^+, measured by the spectrophotometric method, was equal to 9.08 ± 0.05 (n = 3), which is in agreement with literature values [59,60].

As previously described, changes in *diff*log*P* values indicate variations in terms of the multiple interactions and partitioning of procaine in a biphasic system, depending on the counterion. It has been observed that a higher lipophilicity of the charged species ($\log P^I$) is related to a higher ion pair stability, when compared to its corresponding neutral species ($\log P^N$). Other studies demonstrated a clear relationship between the partitioning of ion pairs (lower plateau values $\log P^I$) and the electrolyte concentration of the aqueous phase, influenced by ion species [61,62]. On the other side, variations in terms of $\log P^N$ (higher plateau values) are expected to be negligible, as the neutral specie of the drug should remain predominantly stable and unaffected by the presence of other solutes [63]. However, based on our findings, we noted deviations from this expectation. Moderate differences in $\log P^N$ values can be rationalized by considering a potential residual effects of the counterions, which may indirectly influence the partitioning behavior. Specifically, weak, transient interactions between certain counterions and the neutral species during the partitioning process could lead to shifts in the observed $\log P^N$ values across the series of salts. Additionally, variations in the counterions may alter the microstructure of the octanol phase, potentially affecting its ability to accommodate the neutral form [58]. In this context, if we consider the combination of $\log P^I$ and $\log P^N$ to calculate *diff*log*P*, compounds in which ion pair formation is more favorable with respect to the corresponding neutral species would tend to have smaller *diff*log*P* values compared to those in which ion pair formation is less favorable. As shown in Table 1, the *diff*log*P* values spanned more than one log unit, ranging from 2.50 of PRO-MAE to 3.94 of PRO-CAM. This suggests that the structural variation in the series of 10 procaine counterions prompted a significant variation in the ion pair stability among these compounds. According to the obtained *diff*log*P* increasing scale, three groups of ion pairs with decreasing stability can be identified. Specifically, PRO-MAE and PRO-OX are the two procaine salts allowing a major increase in the relative stability of the ion pair. Indeed, their *diff*log*P* values are equal to 2.50 and 2.52, respectively. Among the other procaine salts, it is possibile to distinguish an intermediate group of salts composed by PRO-MES with a *diff*log*P* of 3.10, and PRO-FUM, PRO-HCl, PRO-BES, PRO-XA and PRO-SUC with a *diff*log*P* around 3.20, which are characterized by an intermediate stability of the ionic couple formed with protonated procaine. Finally, PRO-TOS, PRO-TAR, and PRO-CAM form the least stable ion pairs, with *diff*log*P* values exceeding 3.40.

4.4. Dissolution studies

Dissolution is a test used to determine the *in-vitro* release rate of dosage forms, which is crucial in determining the bioavailability and the therapeutic effectiveness of a drug. The dissolution tests consist of measuring the levels of procaine concentration for the whole set of salts over a certain period of time in two solutions that mimic physiological conditions. In our experiments we employed a phosphate-buffered saline (PBS) at pH 7.4 and an acetate buffer solution pH 4.5. It was also tested a solution of 0.01 N of HCl at pH 2, simulating the highly acidic conditions of the stomach. However, these studies were discontinued due to the observation of procaine degradation in this medium, already evident within the 2-hour time point. The instability of procaine at pH 2 was evidenced by chromatographic analysis, revealing the presence of the main degradation product (PABA). The chromatogram shown in Fig. S45 of the Supplementary Information clearly illustrates this degradation, highlighting the limitations of procaine stability under such harsh acidic conditions. Typically, the extent and kinetics of solution formation are measured over an 8-hour period. However, in this

Table 1
Overview of pKa, lipophilicity parameters and apparent permeability (P_{app}) of procaine salts. $\log P^N$, $\log P^I$, difflogP and pKa were obtained from the fitting of shake-flask logD *vs* pH profiles for each procaine salts, while $\log P_{counterion}$ were sourced from the literature[56].

	Salts	pKa[a]	log*P*^{N}	log*P*^{I}	*diff*log*P*	log*P*$_{counterion}$	$P_{app\ pH\ 4.5}$ (10^{-5} cm/s)	$P_{app\ pH\ 7.4}$ (10^{-5} cm/s)
Reference	PRO-HCl	8.98	1.74	−1.47	3.21	0.25	2.73	2.78
Sulfonates	PRO-MES	9.08	1.95	−1.15	3.10	−0.84	3.54	3.28
	PRO-TOS	9.08	2.03	−1.44	3.47	1.05	6.12	6.37
	PRO-CAM	9.31	2.00	−1.94	3.94	0.59	6.88	6.75
	PRO-BES	8.93	1.16	−2.05	3.21	0.62	4.75	4.86
Carboxylates	PRO-OX	8.75	0.78	−1.74	2.52	−0.69	2.63	2.58
	PRO-MAE	8.75	1.07	−1.42	2.49	−0.42	3.39	3.33
	PRO-XA	8.84	1.78	−1.43	3.21	2.93	8.86	9.84
	PRO-FUM	9.26	1.34	−1.83	3.17	−0.42	3.55	3.77
	PRO-SUC	9.38	1.44	−1.83	3.27	−0.71	3.05	2.83
	PRO-TAR	9.27	1.87	−1.93	3.80	−2.24	5.82	5.75

[a] p*K*a refers to the protonated form of procaine, denoted as protonated procaine cation (PH^+).

experimental study, particular emphasis was placed on the first 2 h (120 min), since no relevant events were observed beyond this timeframe: all the salts remained in solution at constant concentration of 1 mg/mL of procaine, even after 8 h.

The dissolution kinetics of procaine free-base is sluggish, as the concentration varies within the range of 600 μg/mL to 800 μg/mL throughout the experiment. This behavior is attributed to the rapid degradation of the drug. In contrast, all other salts achieve complete dissolution, attaining a steady state of 1 mg/mL in approximately 30 min both at pH 4.5 and 7.4, presumably due to the increased stability and affinity of the PH^+ for the aqueous phase relative to its neutral form. By facilitating quicker and more consistent release rates, the ion pair formation may prevent or mitigate the rapid degradation of procaine, potentially resulting in enhanced drug absorption. By inspection of dissolution profiles of the systems (Fig. 7), it is possible to notice that there are no substantial differences between the salt profiles. Notably, PRO-HCl, PRO-BES, PRO-OX, PRO-CAM, PRO-MAE, PRO-MES, PRO-FUM and PRO-TAR achieve complete dissolution within 5 min. Only PRO-XA, PRO-SUC and PRO-TOS exhibit a relatively slight decrease in dissolution kinetics within the initial 20–30 min, although they ultimately reach their maximum dissolution capacity after 30 min. The maximum measured values exhibit a confidence interval encompassing 1 mg/mL, indicating consistent and reliable dissolution profiles across the salts tested (see Table S7-12 in Supporting Information for detailed mean values and standard deviations).

4.5. Permeability studies

Drug permeability refers to the ability of a pharmaceutical molecule to cross the phospholipid bilayer of the plasma membrane, thus enabling absorption from the site of administration to the site of action, ultimately influencing the bioavailability of a drug. In other words, permeability serves as an indicator of the membrane diffusion and effectiveness by which a drug can permeate a barrier and attain its intended target within the body. Permeability studies of procaine salts were undertaken to investigate the potential influence of salification on the membrane diffusion kinetics of procaine in every system. In this context, Permeapad system was specifically selected to enable a controlled and standardized comparison of the permeability behavior of different procaine salts. By minimizing biological variability, this method allowed for the isolated assessment of counterion-dependent effects on passive membrane permeation, ensuring that the observed differences could be directly attributed to the physicochemical properties of each salt. Its simplicity and reproducibility make it a suitable tool for preliminary permeability ranking studies, providing reliable insights prior to more complex biological evaluations [64,65]. Firstly, the samples were completely dissolved in the respective buffer, in order to guarantee that the permeability experiment was unaffected by the dissolution rate. Afterwards, by monitoring procaine concentration into the acceptor compartment over the time in steady state conditions, calculations of diffusion rate through the membrane gave the apparent permeability (P_{app}) value (reported in the Table 1 along with $\log P_{counterion}$ and *diff*$\log P$), according to Fick's law. For mean and standard deviations values related to P_{app} see Table S14 in Supporting Information, while Figs. S46-47 illustrate the permeability curves, both at pH 4.5 and 7.4.

PRO-HCl is considered the reference system of this investigation, since procaine free-base does not reach the maximum concentration in both acetate and PBS buffer (pH 4.5 and 7.4) and consequently, permeation could not be considered independently from the dissolution rate. Consistent with the dissolution profiles, the permeability values also exhibited similar trends across both pH 4.5 and 7.4, indicating that the permeability behavior of these procaine salts remains relatively stable within this pH range. Notably, the P_{app} values of procaine salts display a remarkable variability, with certain salts demonstrating significantly higher values (as for PRO-XA or PRO-CAM), while others exhibit consistently lower or similar values when compared to the P_{app} value of PRO-HCl (for instance, this is the case of PRO-SUC and PRO-OX). This distinctive behavior, based on the $\log P_{counterion}$ and *diff*$\log P$ of PRO-HCl, effectively classifies the group of 11 salts into two distinct subgroups. A graphic representation of the correlation between permeability and the lipophilicity of the counterion (P_{app} *vs* $\log P_{counterion}$) and between permeability and the stability of the ion pair (P_{app} *vs* *diff*$\log P$) is reported in Fig. 8). The observed variation in permeability among the procaine salts suggest that the differences may be influenced by additional chemical properties of the counterion and possibly also by multiple interactions that procaine may form in solution with other ionic species, directly affecting how effectively the procaine molecule diffuses through the membrane.

In our previous studies performed on benzocaine salts, we demonstrated that permeability was driven by lipophilicity of the counterion and supramolecular interactions[29]. In this work, further descriptors related to the partitioning of the drug within the phospholipid membrane were introduced as parameters with the purpose to establish new correlations with the permeation of procaine and its salts. Assuming that the predominant form of a charged compound in *n*-octanol is the ion pair in which the oppositely charged ions remain closely associated, the *diff*$\log P$ parameter encodes for the free energy of ion pair formation. According to Scherrer [66], four factors account for differences in partitioning between the neutral ($\log P^N$) and charged form ($\log P^I$) of a

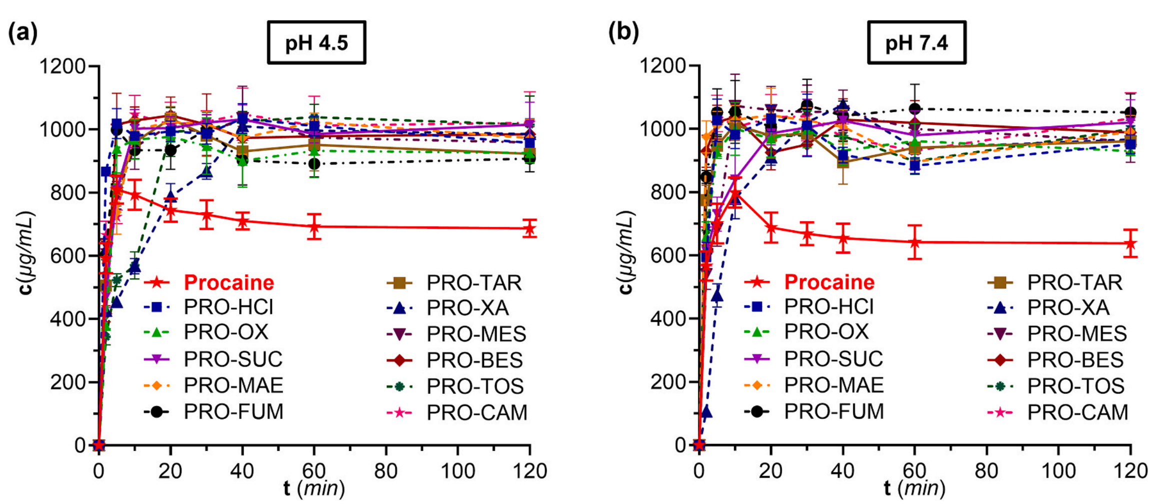

Fig. 7. Dissolution profiles of the procaine salts in the 0–120 min range at (a) pH 4.5 and (b) 7.4.

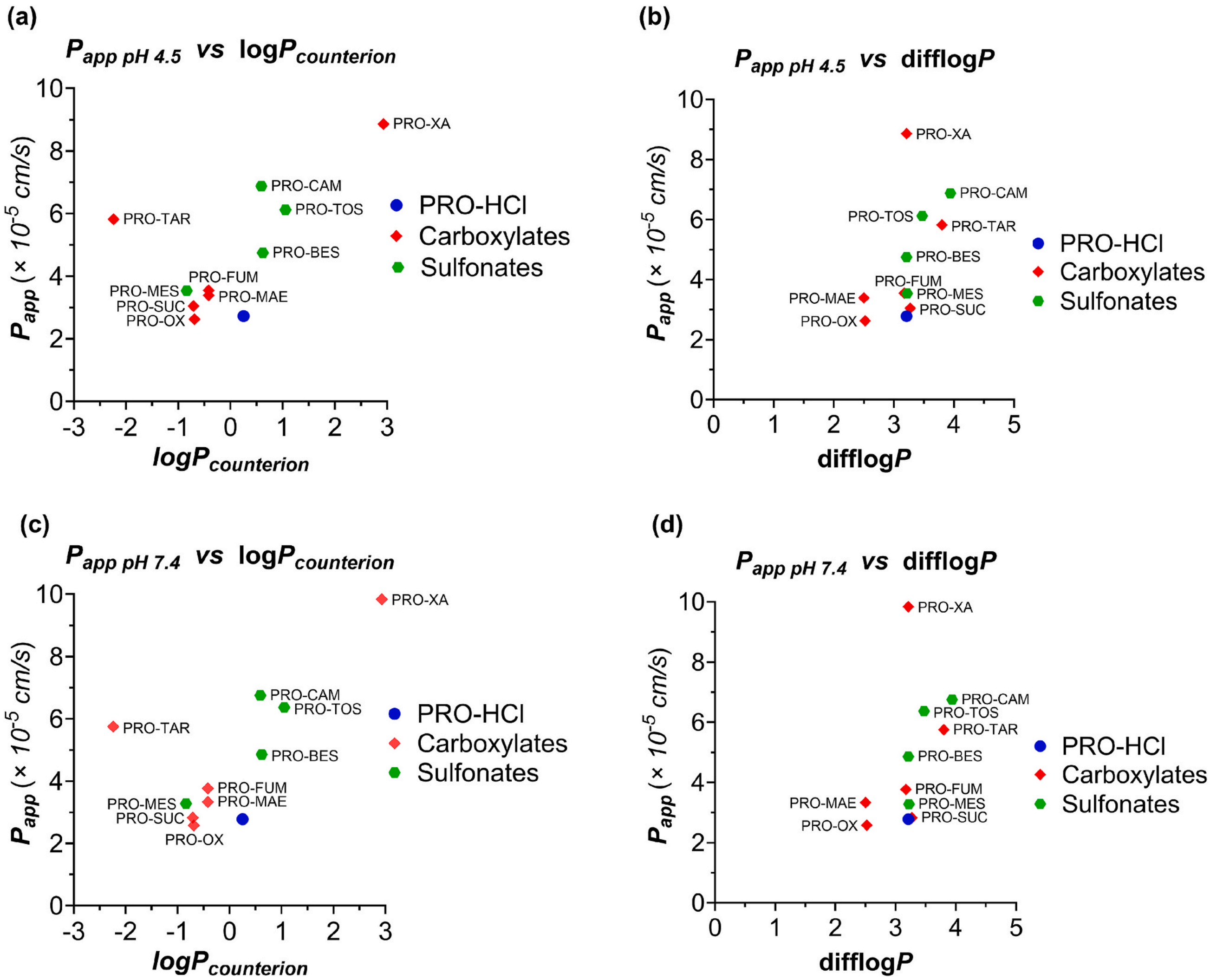

Fig. 8. Visual exploration of the relationships between permeability (P_{app}) and the lipophilicity parameters (difflogP and $logP_{counterion}$) for the organic salts of procaine. The top panels show the correlations of (a) P_{app} *vs* $logP_{counterion}$ and (b) P_{app} *vs* difflogP for pH 4.5, while the bottom panels illustrate the same correlations for pH 7.4 (b and c).

compound: its p*K*a; its chemical class; the steric hindrance around the charge centers; hydrogen bond donor and acceptor groups near the charge center. Our purpose was to search for correlation between lipophilicity descriptors (logP^N, logP^I, log$P_{counterion}$, *diff*log*P*), p*K*a and *in-vitro* permeability, expressed by P_{app} values (as visually illustrated by the correlation matrix reported in Fig. 9 of the next paragraph and outlined in Table 1). This focus stems from the historically limited exploration of lipophilicity of ionizable compounds and the influence of charged microspecies on membrane penetration, largely due to the challenges in reliably measuring the partition coefficients of ionic forms [67].

4.6. Analysis of structure–property relationships

A comprehensive analysis of the interactions occurring between the procaine molecule and the surrounding entities (both anions and symmetry-related cations), combined with p*K*a and our lipophilicity descriptors allow us to examine how the counterion influence properties of dissolution rate and permeability profiles. Specifically, our dissolution studies revealed that procaine salts exhibit a generally faster dissolution rate compared to the procaine free-base, which shows a tendency to degrade over time. Consequently, our primary focus in the structure–property relationship analysis shifts predominantly towards permeability, a parameter that demonstrates more pronounced variations among the procaine salts. This choice reflects the inherent complexity in interpreting salt permeability, a phenomenon that remains a subject of active investigation and debate within the field [68].

Structurally, the analysis of the Hirshfeld surfaces elucidated that hydrogen bonds are the dominant intermolecular forces between the protonated procaine cation and neighboring species (carboxylate or sulfonate anions, and symmetry-related cations) in the solids and, in general, all the salts are structurally organized in similar arrangements; the difference in the properties of interest can be investigated through the analysis of the molecular structures of the counterions, which affect properties in solution of the salts. In an attempt to explore the interplay between counterion structure, lipophilicity, and permeability, we integrated *diff*log*P* with the other fitted lipophilicity parameters (logP^N, logP^I), the lipophilicity of the counterion (log$P_{counterion}$), and permeability (P_{app}) assessed at pH 4.5 and 7.4, in a unique matrix. The resulting full correlation plot in Fig. 9 provides a clear visualization of the Pearson correlation analysis, allowing for a detailed examination of how counterion selection impacts these crucial properties, ultimately affecting permeability. A color and size-coded scheme was used to highlight these relationships: blue circles indicate positive correlations, while red circles represent negative correlations, with the intensity and size reflecting the correlation strength. In this analysis, we observed that *diff*log*P* was significantly correlated with the lipophilicity of the neutral

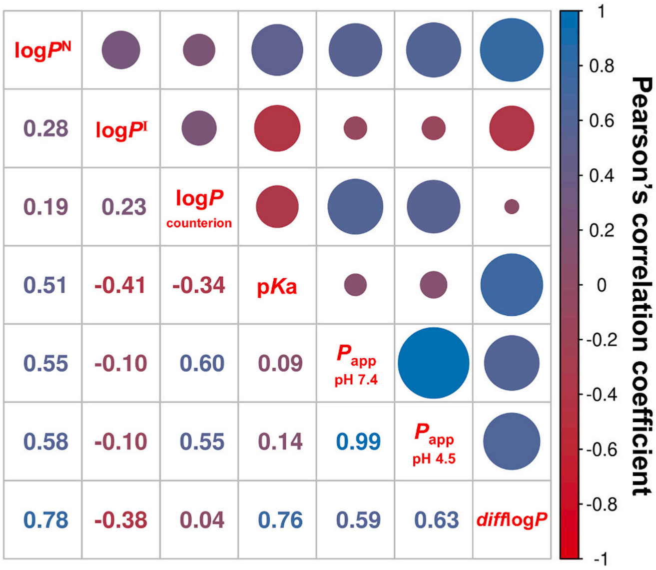

Fig. 9. The full correlation plot represents a visual inspection of Pearson's correlation analysis considering couples of lipophilic parameters, including the whole set of variables considered to describe the permeability (P_{app}) of procaine salts, both measured at pH 4.5 and 7.4 ($P_{app\ pH\ 4.5}$ and $P_{app\ pH\ 7.4}$). In the upper panel, the size of the circle is proportional to the intensity of the correlation. In the lower panel of the plot, the actual figure of the Pearson's correlation is included for each pair of parameters. Colors reflect the Pearson's correlation coefficient reported on the right side of the image.

form logP^N (Pearson's coefficient $r = 0.78$; $p < 0.05$) and slightly inversely correlated with logP^I of the ionic couple ($r = -0.38$). Interestingly, *diff*log*P* was not correlated with log$P_{counterion}$ ($r = 0.10$). This lack of correlation suggests that the lipophilicity of the counterion does not significantly influence the stability of an ion pair (encoded in the *diff*log*P* value).

Furthermore, a strong positive correlation was observed between $P_{app\ pH\ 4.5}$ and $P_{app\ pH\ 7.4}$ (correlation coefficient of 0.99), indicating that the permeability of the procaine salts remains largely consistent across this pH range.

Building upon the observed correlations between *diff*log*P* and lipophilicity, we further investigated the relationship between these parameters and permeability. Remarkably, a moderate positive correlation between permeability and *diff*log*P* was observed (0.63 or 0.59, respectively considering $P_{app\ pH\ 4.5}$ and $P_{app\ pH\ 7.4}$), alongside a similar positive correlation between permeability and log$P_{counterion}$ (approximately 0.60), as depicted in Fig. 8). Interestingly, while P_{app} appears to exhibit a relationship with *diff*log*P*, it does not show any dependence on p*K*a (around 0.1), despite the latter parameter demonstrates a clear correlation with *diff*log*P*. It is evident that, in line with our previous work on benzocaine salts [29], log$P_{counterion}$ appears to be one of the main factors influencing the permeability of the various procaine salts tested. Indeed, sulfonates such as BES, CAM, TOS and also XA generally promote higher permeability, showing ranging from 40 % to 70 % compared to PRO-HCl. On the contrary, carboxylates like OX, MAE, FUM, SUC and MES result in more limited diffusion through the lipid membrane. Notably, PRO-XA deviates from the trend of carboxylates limiting permeability, likely due to its higher log$P_{counterion}$ among the carboxylic acids used, which promote permeation of the membrane [63]. Another salt that deviates from this trend is PRO-TAR. Tartrate is the counterion with the lowest log$P_{counterion}$ among the carboxylic acid used, beside to be the only counterion that generate a bis-deprotonated salt. Eventually, mesylate, despite being a sulfonate, shows hydrophilicity (low log$P_{counterion}$) comparable to that of carboxylic acids, which likely accounts for its permeability behavior, more similar to that of the carboxylate salts.

Given these observations, the log$P_{counterion}$ alone cannot fully explain the complexity of permeability, suggesting that additional factors must be involved. Since ion pair formation distinguishes a salt from its parent drug, *diff*log*P* (which reflects the collective interactions of procaine for each salt during the partitioning) emerges as a potentially valuable descriptor. *diff*log*P* was expected to show an inverse relationship with permeability, since the more stable the ion pair is, the more its overall hydrophobic character is expected to be enhanced, potentially leading to increased permeability of the salt through the membrane [69]. However, as can be seen, the less permeable salts are characterized by a lower *diff*log*P* (PRO-OX, PRO-MAE), while the more permeable salts have a much higher *diff*log*P* (PRO-XA, PRO-CAM, PRO-BES, and PRO-TOS). At first glance, looking at the log*P* of the counterions of these salts, it seems that, in this case as well, the log*P* of the counterion plays a crucial role in promoting permeability. If an ion pair is highly stable but paired with a highly hydrophilic counterion, its stability may actually hinder its passage through biological membranes, as observed with PRO-OX and PRO-MAE.

Another possible explanation for this unusual behavior could be found in the study by Austin et al. [70], which highlights the differences in *diff*log*P* values between an *n*-octanol/water system and a system composed by a lipid phase with liposomes and water. This study particularly emphasizes the behavior of primary, secondary, and tertiary amines in these two systems. Essentially, it shows that for this type of molecule, the ion pair is less relevant in partitioning into the lipid phase. Specifically, amines tend to form numerous interactions with biological membranes, making them highly compatible with this type of environment. A clear example of this behavior is evident in Austin's work, where the *diff*log$P_{oct/wat}$ of a primary amine differs significantly from the *diff*log$P_{lip/wat}$ (3 *vs* 0.29). Such findings suggest that more stable ion pairs could hinder the ability of procaine (a tertiary amine) to partition into biological membranes, whereas less stable ion pairs allow for easier distribution through the phospholipid bilayer. According to this hypotesis, we can suppose that ion pair survives only in the extracellular environment and dissociates at the membrane interface, where procaine must lose a proton to cross the lipid bilayer to allow passive permeability as a neutral specie (as procaine free-base). This is plausible given that protonation and deprotonation equilibria are likely to differ in the hydrophobic environment of the water/membrane interface [71]. A stronger correlation of logP^N with P_{app} compared to logP^I supports this hypothesis, as illustrated in Fig. 9. Specifically, logP^N demostrates a moderate correlation with P_{app} (correlation coefficient of 0.55–0.58 across the two physiological pH), whereas logP^I is barely correlated with P_{app}, with a coefficient of -0.10. Such results highlights that, indeed, passive membrane permeation may be more influenced by the lipophilicity of procaine in its neutral form than by its lipophilicity in the ionized form (logP^I), as the canonical model assumes [71].

5. Conclusion

In this study, we successfully synthesized and characterized eleven procaine salts with both carboxylic and sulfonic acids, aiming to explore their impact on dissolution rate and permeability and potentially overcome the swift degradation of the drug.

The dissolution rate of the procaine salts is consistent across the different systems in both the buffered solution tested at pH 4.5 and 7.4, remaining stable and dissolved for up to 8 h. The establishment of interactions between the two components of these procaine salts introduces a dynamic element that allows for the modulation of the properties of the parent drug, potentially maintaining a more stable blood concentration over an extended period compared to procaine free-base. On the other side, intriguing distinctions emerge in the permeability profiles and to understand this behavior, physico-chemical descriptors were introduced, with particular attention to lipophilicity parameters, namely log$P_{counterion}$, *diff*log*P*, logP^N and logP^I. Notably, sulfonate salts, characterized by higher log$P_{counterion}$ and lower ion pair stability (as indicated by *diff*log*P*), exhibited enhanced permeability compared to carboxylate salts, which displayed lower $\log P_{\text{counterion}}$ and higher ion pair stability. These insights, coupled with the observation that permeability is also moderately correlated with the lipophilicity of the neutral procaine form ($\log P^{N}$) rather than the ionic form ($\log P^{I}$), support the hypothesis of the canonical model that the passive permeability of a drug may be primarily governed by its neutral species. Indeed, as also proposed by Yue and co-workers [69], an ion pair does not necessarily cross the membrane as a self-assembled ionic complex with its counterion. Instead, it may be affected by the distinct microenvironment at the water/membrane interface or within the transmembrane compartment. In such contexts, the ion pair could dissociate, triggering dynamic deprotonation effects that alter and shift the equilibrium, allowing the drug to permeate the membrane in its neutral form. Furthermore, the consistent dissolution and permeability behaviors of these salts across a physiologically relevant pH range from 4.5 to 7.4 reinforce their potential as reliable drug delivery systems capable of withstanding varying environmental conditions within a 3-unit pH range.

In conclusion, our study provides a comprehensive understanding of how counterion selection influences the dissolution and permeability of procaine salts. The observed trends, particularly the enhanced permeability in the case of sulfonate salts and the pH stability of all salts, offer valuable insights for the design of more effective procaine-based drug delivery systems. Based on our current data, sulfonate salts appear particularly promising for applications where enhanced permeability and drug delivery in a pH range between 4.5 and 7.4 are crucial.

CRediT authorship contribution statement

Paola Disisto: Writing – original draft, Investigation, Formal analysis, Conceptualization, Visualization. **Laura Baraldi:** Investigation, Formal analysis, Conceptualization. **Luca Fornasari:** Investigation, Formal analysis. **Irene Bassanetti:** Writing – review & editing. **Valentina Mileo:** Writing – review & editing. **Francesco Castagnini:** Writing – review & editing, Investigation, Formal analysis. **Francesca Ferlenghi:** Investigation, Formal analysis. **Pietro Franceschi:** Visualization, Formal analysis. **Alessia Bacchi:** Writing – review & editing. **Luciano Marchiò:** Writing – review & editing, Supervision, Project administration, Investigation.

Declaration of competing interest

The authors declare that they have no known competing financial interests or personal relationships that could have appeared to influence the work reported in this paper.

Acknowledgment

Chiesi Farmaceutici SpA is acknowledged for funding this work and for the support of the D8 Venture X-ray equipment. This work also benefited from the equipment and framework of the COMP-HUB and COMP-R Initiatives, funded by the 'Departments of Excellence' program of the Italian Ministry for University and Research (MIUR, 2018-2022 and MUR, 2023-2027). Chiesi Farmaceutici SpA and the Italian Ministry of University and Research are acknowledged for a PhD scholarship, M.D. 117/2023 (P.D.).

Appendix A. Supplementary material

Supplementary data to this article can be found online at https://doi.org/10.1016/j.ejpb.2025.114758.

Data availability

Data will be made available on request.

References

[1] D. Gradinaru, A. Ungurianu, D. Margina, M. Moreno-Villanueva, A. Bürkle, Procaine - the controversial geroprotector candidate: new insights regarding its molecular and cellular effects, Oxid. Med. Cell. Longev. 2021 (2021) 1–18, https://doi.org/10.1155/2021/3617042.
[2] Yu. Siyi, B. Wang, J. Zhang, K. Fang, The development of local anesthetics and their applications beyond anesthesia, Int. J. Clin. Exp. Med. 12 (2019) 13203–13220.
[3] S. Johnson, Cocaine to procaine: an unexpected history of local anaesthesia, Biomed J Sci Tech Res 7 (2018), https://doi.org/10.26717/BJSTR.2018.07.001467.
[4] R.A. Goldstein, C. DesLauriers, A. Burda, K. Johnson-Arbor, Cocaine: history, social implications, and toxicity: a review, Semin. Diagn. Pathol. 26 (2009) 10–17, https://doi.org/10.1053/j.semdp.2008.12.001.
[5] J.S. Jacob, A.L. Kovac, Procaine and local anesthetic toxicity, Reg. Anesth. Pain Med. 42 (2017) 760–763, https://doi.org/10.1097/AAP.0000000000000664.
[6] F.V. Salinas, K. Malik, H.T. Benzon, Local anesthetics for regional anesthesia and pain management, in: Raj's Practical Management of Pain, Elsevier, 2008: pp. 811–838. doi: 10.1016/B978-032304184-3.50047-9.
[7] J. Shah, E.G. Votta-Velis, A. Borgeat, New local anesthetics, Best Pract. Res. Clin. Anaesthesiol. 32 (2018) 179–185, https://doi.org/10.1016/j.bpa.2018.06.010.
[8] D.E. Becker, K.L. Reed, Essentials of local anesthetic pharmacology., Anesth Prog 53 (2006) 98–108; quiz 109–10. doi: 10.2344/0003-3006(2006)53[98:EOLAP]2.0.CO;2.
[9] Y.-H. Wang, D.-R. Wang, J.-Y. Liu, J. Pan, Local anesthesia in oral and maxillofacial surgery: a review of current opinion, J Dent Sci 16 (2021) 1055–1065, https://doi.org/10.1016/j.jds.2020.12.003.
[10] D.E. Becker, K.L. Reed, Local anesthetics: review of pharmacological considerations, Anesth. Prog. 59 (2012) 90–102, https://doi.org/10.2344/0003-3006-59.2.90.
[11] Y. He, L. Qin, Y. Huang, C. Ma, Advances of nano-structured extended-release local anesthetics, Nanoscale Res. Lett. 15 (2020) 13, https://doi.org/10.1186/s11671-019-3241-2.
[12] P. Lirk, S. Picardi, M.W. Hollmann, Local anaesthetics, Eur. J. Anaesthesiol. 31 (2014) 575–585, https://doi.org/10.1097/EJA.0000000000000137.
[13] K. El-Boghdadly, A. Pawa, K.J. Chin, Local anesthetic systemic toxicity: current perspectives, Local Reg Anesth 11 (2018) 35–44, https://doi.org/10.2147/LRA.S154512.
[14] A. Tavasli, B. Kocaaga, F.S. Guner, Development of procaine loaded transdermal patches based on biopolymer pectin, castor oil, and polyethylene glycol for controllable drug release studies and their characterizations, ChemistrySelect 8 (2023), https://doi.org/10.1002/slct.202301115.
[15] S. Rodoplu, B.E. Celik, B. Kocaaga, C. Ozturk, S. Batirel, D. Turan, F.S. Guner, Dual effect of procaine-loaded pectin hydrogels: pain management and in vitro wound healing, Polym. Bull. 78 (2021) 2227–2250, https://doi.org/10.1007/s00289-020-03210-7.
[16] S. Beiranvand, A. Eatemadi, A. Karimi, New updates pertaining to drug delivery of local anesthetics in particular bupivacaine using lipid nanoparticles, Nanoscale Res. Lett. 11 (2016) 307, https://doi.org/10.1186/s11671-016-1520-8.
[17] H. Ma, Z. Pan, B. Lai, C. Zan, H. Liu, Recent research advances in nano-based drug delivery systems for local anesthetics, Drug Des. Devel. Ther. 17 (2023) 2639–2655, https://doi.org/10.2147/DDDT.S417051.
[18] M. Ji, G. Liu, Y. Cui, P. Zhao, Safety and efficacy concerns of modern strategies of local anesthetics delivery, 3 Biotech 10 (2020) 333, https://doi.org/10.1007/s13205-020-02309-y.
[19] L. Visai, L. Zorzetto, P. Brambilla, N. Bloise, M. De Gregori, L. Cobianchi, M. Allegri, P. Petrini, E. Marcello, A. Peloso, From micro- to nanostructured implantable device for local anesthetic delivery, Int. J. Nanomed. (2016) 2695, https://doi.org/10.2147/IJN.S99028.
[20] J.E. Usubiaga, F. Moya, J.A. Wikinski, R. Wikinski, L.E. Usubiaga, Relationship between the passage of local anaesthetics across the blood-brain barrier and their effects on the central nervous system, Br. J. Anaesth. 39 (1967) 943–947, https://doi.org/10.1093/bja/39.12.943.
[21] D. Gupta, D. Bhatia, V. Dave, V. Sutariya, S. Varghese Gupta, Salts of therapeutic agents: chemical, physicochemical, and biological considerations, Molecules 23 (2018), https://doi.org/10.3390/molecules23071719.
[22] P. Guerrieri, K. Jarring, L.S. Taylor, Impact of counterion on the chemical stability of crystalline salts of procaine, J. Pharm. Sci. 99 (2010) 3719–3730, https://doi.org/10.1002/jps.22009.
[23] M. Cristofoli, C.-P. Kung, J. Hadgraft, M.E. Lane, B.C. Sil, Ion pairs for transdermal and dermal drug delivery: a review, Pharmaceutics 13 (2021) 909, https://doi.org/10.3390/pharmaceutics13060909.
[24] B. Dutton, A. Woods, R. Sadler, D. Prime, D.J. Barlow, B. Forbes, S.A. Jones, Using polar ion-pairs to control drug delivery to the airways of the lungs, Mol. Pharm. 17 (2020) 1482–1490, https://doi.org/10.1021/acs.molpharmaceut.9b01166.
[25] X. Ji, D. Wu, C. Li, J. Li, Q. Sun, D. Chang, Q. Yin, L. Zhou, C. Xie, J. Gong, W. Chen, Enhanced solubility, dissolution, and permeability of abacavir by salt and cocrystal formation, Cryst. Growth Des. 22 (2022) 428–440, https://doi.org/10.1021/acs.cgd.1c01051.
[26] S.P. Gopi, M. Banik, G.R. Desiraju, New cocrystals of hydrochlorothiazide: optimizing solubility and membrane diffusivity, Cryst. Growth Des. 17 (2017) 308–316, https://doi.org/10.1021/acs.cgd.6b01540.
[27] P. Sanphui, V.K. Devi, D. Clara, N. Malviya, S. Ganguly, G.R. Desiraju, Cocrystals of hydrochlorothiazide: solubility and diffusion/permeability enhancements through drug–coformer interactions, Mol. Pharm. 12 (2015) 1615–1622, https://doi.org/10.1021/acs.molpharmaceut.5b00020.

[28] A.K. Nangia, G.R. Desiraju, Crystal engineering: an outlook for the future, Angew. Chem. Int. Ed. 58 (2019) 4100–4107, https://doi.org/10.1002/anie.201811313.
[29] L. Baraldi, I. Bassanetti, F. Amadei, A. Bacchi, L. Marchiò, Salts and cocrystals of benzocaine with increased dissolution rate and permeability open new avenues for enhancing the duration of action, Cryst. Growth Des. 24 (2024) 2157–2167, https://doi.org/10.1021/acs.cgd.3c01488.
[30] S.S. Bharate, Carboxylic acid counterions in FDA-approved pharmaceutical salts, Pharm. Res. 38 (2021) 1307–1326, https://doi.org/10.1007/s11095-021-03080-2.
[31] S.S. Bharate, Modulation of biopharmaceutical properties of drugs using sulfonate counterions: a critical analysis of FDA-approved pharmaceutical salts, J Drug Deliv Sci Technol 66 (2021) 102913, https://doi.org/10.1016/j.jddst.2021.102913.
[32] P.H. Stahl, C.G. Wermuth, Handbook of pharmaceutical salts: properties, selection, and use, Chemistry International – Newsmagazine for IUPAC 24 (2002), https://doi.org/10.1515/ci.2002.24.3.20a.
[33] P. Guerrieri, A.C.F. Rumondor, T. Li, L.S. Taylor, Analysis of relationships between solid-state properties, counterion, and developability of pharmaceutical salts, AAPS PharmSciTech 11 (2010) 1212–1222, https://doi.org/10.1208/s12249-010-9499-4.
[34] K. Mazák, B. Noszál, Drug delivery: a process governed by species-specific lipophilicities, Eur. J. Pharm. Sci. 62 (2014) 96–104, https://doi.org/10.1016/j.ejps.2014.05.017.
[35] A. Malvezzi, A.T. do Amaral, Ion pair stabilization effects on a series of procaine structural analogs, Eur. J. Pharm. Sci. 41 (2010) 631–635, doi: 10.1016/j.ejps.2010.09.003.
[36] G. Caron, F. Reymond, P.-A. Carrupt, H.H. Girault, B. Testa, Combined molecular lipophilicity descriptors and their role in understanding intramolecular effects, Pharm. Sci. Technol. Today 2 (1999) 327–335, https://doi.org/10.1016/S1461-5347(99)00180-7.
[37] R.A. Scherrer, Biolipid p K_a Values and the Lipophilicity of Ampholytes and Ion Pairs, in: Pharmacokinetic Optimization in Drug Research, Wiley, 2001: pp. 351–381. doi: 10.1002/9783906390437.ch20.
[38] Y. Marcus, G. Hefter, Ion pairing, Chem. Rev. 106 (2006) 4585–4621, https://doi.org/10.1021/cr040087x.
[39] N.F.A. van der Vegt, K. Haldrup, S. Roke, J. Zheng, M. Lund, H.J. Bakker, Water-mediated ion pairing: occurrence and relevance, Chem. Rev. 116 (2016) 7626–7641, https://doi.org/10.1021/acs.chemrev.5b00742.
[40] H.J. Davis, M.T. Mihai, R.J. Phipps, Ion Pair-directed regiocontrol in transition-metal catalysis: a meta-selective C–H borylation of aromatic quaternary ammonium salts, J. Am. Chem. Soc. 138 (2016) 12759–12762, https://doi.org/10.1021/jacs.6b08164.
[41] G.M. Sheldrick, SADABS-2008/1—Bruker AXS Area Detector Scaling and Absorption Correction, Bruker AXS: Madison, WI, USA (2008).
[42] G.M. Sheldrick, *SHELXT* – Integrated space-group and crystal-structure determination, Acta Crystallogr A Found Adv 71 (2015) 3–8, https://doi.org/10.1107/S2053273314026370.
[43] G.M. Sheldrick, Crystal structure refinement with *SHELXL*, Acta Crystallogr C, Struct. Chem. 71 (2015) 3–8, https://doi.org/10.1107/S2053229614024218.
[44] O.V. Dolomanov, L.J. Bourhis, R.J. Gildea, J.A.K. Howard, H. Puschmann, *OLEX2*: a complete structure solution, refinement and analysis program, J. Appl. Cryst. 42 (2009) 339–341, https://doi.org/10.1107/S0021889808042726.
[45] P.R. Spackman, M.J. Turner, J.J. McKinnon, S.K. Wolff, D.J. Grimwood, D. Jayatilaka, M.A. Spackman, *CrystalExplorer* : a program for Hirshfeld surface analysis, visualization and quantitative analysis of molecular crystals, J. Appl. Cryst. 54 (2021) 1006–1011, https://doi.org/10.1107/S1600576721002910.
[46] M.A. Spackman, D. Jayatilaka, Hirshfeld surface analysis, CrstEngComm 11 (2009) 19–32, https://doi.org/10.1039/B818330A.
[47] A.-C. Jacobsen, S. Nielsen, M. Brandl, A. Bauer-Brandl, Drug permeability profiling using the novel Permeapad® 96-well plate, Pharm. Res. 37 (2020) 93, https://doi.org/10.1007/s11095-020-02807-x.
[48] M.M. Tzanova, E. Randelov, P.C. Stein, M. Hiorth, M.P. di Cagno, Towards a better mechanistic comprehension of drug permeation and absorption: Introducing the diffusion-partitioning interplay, Int. J. Pharm. 608 (2021) 121116, https://doi.org/10.1016/j.ijpharm.2021.121116.
[49] A. Avdeef, J.E.A. Comer, S.J. Thomson, pH-Metric log P. 3. Glass electrode calibration in methanol-water, applied to pKa determination of water-insoluble substances, Anal Chem 65 (1993) 42–49. doi: 10.1021/ac00049a010.
[50] R.I. Allen, K.J. Box, J.E.A. Comer, C. Peake, K.Y. Tam, Multiwavelength spectrophotometric determination of acid dissociation constants of ionizable drugs, J. Pharm. Biomed. Anal. 17 (1998) 699–712, https://doi.org/10.1016/S0731-7085(98)00010-7.
[51] C. Mongay, V. Cerda, A britton-Robinson buffer of known ionic strength, Anal. Chim. 64 (1974) 409–412.
[52] A. Avdeef, Assessment of distribution-pH profiles, In (1996) 109–139, https://doi.org/10.1002/9783527614998.ch7.
[53] R Core Team, R: A language and environment for statistical computing. R Foundation for Statistical Computing, (2024). Available from https://www.R-project.org/.
[54] T. Wei, V. Simko, R package "corrplot": Visualization of a Correlation Matrix, (2024). Available from https://github.com/taiyun/corrplot.
[55] R. Beall, J. Herdklotz, R.L. Sass, Molecular properties of local anesthetics: The crystal structure of procaine hydrochloride, Biochem. Biophys. Res. Commun. 39 (1970) 329–334, https://doi.org/10.1016/0006-291X(70)90580-2.
[56] S. Kim, J. Chen, T. Cheng, A. Gindulyte, J. He, S. He, Q. Li, B.A. Shoemaker, P.A. Thiessen, B. Yu, L. Zaslavsky, J. Zhang, E.E. Bolton, PubChem 2023 update, Nucleic Acids Res 51 (2023) D1373–D1380. doi: 10.1093/nar/gkac956.
[57] J.P. Guthrie, Hydrolysis of esters of oxy acids: p K_a values for strong acids; Brønsted relationship for attack of water at methyl; free energies of hydrolysis of esters of oxy acids; and a linear relationship between free energy of hydrolysis and p K_a holding over a range of 20 p K units, Can. J. Chem. 56 (1978) 2342–2354, https://doi.org/10.1139/v78-385.
[58] A. Avdeef, Absorption and drug development: solubility, permeability, and charge state, Wiley (2012), https://doi.org/10.1002/9781118286067.
[59] Donald Cairns, Essentials of Pharmaceutical Chemistry, 4th edition, UK, 2012.
[60] B.G. Covino, Pharmacology of local anaesthetic agents, Br. J. Anaesth. 58 (1986) 701–716, https://doi.org/10.1093/bja/58.7.701.
[61] P.I. Nagy, K. Takács-Novák, Theoretical and experimental study on ion-pair formation and partitioning of organic salts in octanol/water and dichloromethane/water systems, J. Am. Chem. Soc. 122 (2000) 6583–6593, https://doi.org/10.1021/ja000355i.
[62] Z. Disdier, S. Savoye, R.V.H. Dagnelie, Effect of solutes structure and pH on the n-octanol/water partition coefficient of ionizable organic compounds, Chemosphere 304 (2022) 135155, https://doi.org/10.1016/j.chemosphere.2022.135155.
[63] K. Takács-Novák, G. Szász, Ion-pair partition of quaternary ammonium drugs: the influence of counter ions of different lipophilicity, size, and flexibility, Pharm. Res. 16 (1999) 1633–1638, https://doi.org/10.1023/A:1018977225919.
[64] A.-C. Jacobsen, S. Visentin, C. Butnarasu, P.C. Stein, M.P. di Cagno, Commercially available cell-free permeability tests for industrial drug development: increased sustainability through reduction of in vivo studies, Pharmaceutics 15 (2023) 592, https://doi.org/10.3390/pharmaceutics15020592.
[65] R. Hayeshi, C. Hilgendorf, P. Artursson, P. Augustijns, B. Brodin, P. Dehertogh, K. Fisher, L. Fossati, E. Hovenkamp, T. Korjamo, C. Masungi, N. Maubon, R. Mols, A. Müllertz, J. Mönkkönen, C. O'Driscoll, H.M. Oppers-Tiemissen, E.G. E. Ragnarsson, M. Rooseboom, A.-L. Ungell, Comparison of drug transporter gene expression and functionality in Caco-2 cells from 10 different laboratories, Eur. J. Pharm. Sci. 35 (2008) 383–396, https://doi.org/10.1016/j.ejps.2008.08.004.
[66] R.A. Scherrer, S.F. Donovan, Automated potentiometric titrations in KCl/water-saturated octanol: method for quantifying factors influencing ion-pair partitioning, Anal. Chem. 81 (2009) 2768–2778, https://doi.org/10.1021/ac802729k.
[67] K. Mazák, B. Noszál, Advances in microspeciation of drugs and biomolecules: Species-specific concentrations, acid-base properties and related parameters, J. Pharm. Biomed. Anal. 130 (2016) 390–403, https://doi.org/10.1016/j.jpba.2016.03.053.
[68] A. Samie, H. Alavian, A perspective on the permeability of cocrystals/organic salts of oral drugs, Mol. Pharm. 21 (2024) 4860–4911, https://doi.org/10.1021/acs.molpharmaceut.4c00786.
[69] N. Samiei, A. Shafaati, A. Zarghi, H.R. Moghimi, S.M. Foroutan, Enhancement and in vitro evaluation of amifostine permeation through artificial membrane (PAMPA) via ion pairing approach and mechanistic selection of its optimal counter ion, Eur. J. Pharm. Sci. 51 (2014) 218–223, https://doi.org/10.1016/j.ejps.2013.10.002.
[70] R.P. Austin, A.M. Davis, C.N. Manners, Partitioning of ionizing molecules between aqueous buffers and phospholipid vesicles, J. Pharm. Sci. 84 (1995) 1180–1183, https://doi.org/10.1002/jps.2600841008.
[71] Z. Yue, C. Li, G.A. Voth, J.M.J. Swanson, Dynamic protonation dramatically affects the membrane permeability of drug-like molecules, J. Am. Chem. Soc. 141 (2019) 13421–13433, https://doi.org/10.1021/jacs.9b04387.